

# Electron heated target temperature measurements in petawatt laser experiments based on extreme ultraviolet imaging and spectroscopy<sup>a)</sup>

T. Ma,<sup>1,2</sup> F. N. Beg,<sup>1</sup> A. G. MacPhee,<sup>2</sup> H.-K. Chung,<sup>2</sup> M. H. Key,<sup>2</sup> A. J. Mackinnon,<sup>2</sup> P. K. Patel,<sup>2</sup> S. Hatchett,<sup>2</sup> K. U. Akli,<sup>3</sup> R. B. Stephens,<sup>3</sup> C. D. Chen,<sup>4</sup> R. R. Freeman,<sup>5</sup> A. Link,<sup>5</sup> D. T. Offermann,<sup>5</sup> V. Ovchinnikov,<sup>5</sup> and L. D. Van Woerkom<sup>5</sup>

<sup>1</sup>*Department of Mechanical and Aerospace Engineering, University of California-San Diego, 9500 Gilman Drive, La Jolla, California 92093-0417, USA*

<sup>2</sup>*Lawrence Livermore National Laboratory, 7000 East Ave., Livermore, California 94550, USA*

<sup>3</sup>*General Atomics, San Diego, California 92186, USA*

<sup>4</sup>*Plasma Science Fusion Center, Massachusetts Institute of Technology, Cambridge, Massachusetts 02139, USA*

<sup>5</sup>*College of Mathematical and Physical Sciences, The Ohio State University, 425 Stillman Hall, Columbus, Ohio 43210-1123, USA*

(Presented 12 May 2008; received 11 May 2008; accepted 7 July 2008; published online 31 October 2008)

Three independent methods (extreme ultraviolet spectroscopy, imaging at 68 and 256 eV) have been used to measure planar target rear surface plasma temperature due to heating by hot electrons. The hot electrons are produced by ultraintense laser-plasma interactions using the 150 J, 0.5 ps Titan laser. Soft x-ray spectroscopy in the 50–400 eV region and imaging at the 68 and 256 eV photon energies give a planar deuterated carbon target rear surface pre-expansion temperature in the 125–150 eV range, with the rear plasma plume averaging a temperature approximately 74 eV.

© 2008 American Institute of Physics. [DOI: [10.1063/1.2965260](https://doi.org/10.1063/1.2965260)]

## I. INTRODUCTION

The use of soft x-ray imaging and spectroscopy is a useful tool to measure the magnitude and spatial distribution of energy deposition by thermal electrons in laser-plasma interactions.<sup>1–4</sup> When an ultraintense laser hits a solid target, a large flux of energetic electrons are created which then heat the material, and among the radiation generated is a thermal Planckian emission spectrum peaking in the extreme ultraviolet (XUV) to soft x-ray spectral region. This radiation intensity varies rapidly with temperature, and thus time-integrated imaging, as well as spectroscopic resolution of the radiation offers an excellent tool to determine plasma temperatures. The aim of this work is to compare three different methods for determining the thermal temperature—two based on two-dimensional monochromatic XUV imaging, and the other on one-dimensional spatially resolved spectroscopic measurements—under short-pulse, high intensity laser irradiation conditions.

## II. EXPERIMENT

Experiments were carried out on the Titan laser at the Lawrence Livermore National Laboratory. The 150 J, 0.5 ps,  $\lambda=1053$  nm laser is used to illuminate 25  $\mu\text{m}$  thick,  $1 \times 1$  mm<sup>2</sup> deuterated carbon (CD) plastic planar targets under a variety of irradiation conditions (varying on-target laser intensities by changing the focal spot size). The Planckian radiation emitted when the target heats up is captured by a

flat-field spectrometer<sup>3,4</sup> (FFS) which records spectra in the 50–400 eV (30–250 Å wavelength) range and two XUV imagers,<sup>1,2</sup> one operating at the 68 eV photon energy, the other at the 256 eV photon energy. The experimental setup is illustrated in Fig. 1.

The FFS consists of a 1200 lines/mm concave diffraction grating set to a glancing angle of 4.6°. The use of such a concave grating with variable line spacing allows the imaging of the spectrum on a flat plane instead of on the Rowland circle. Thus, the spectrum can be recorded on a flat detector, and here a vacuum charge coupled device (CCD) with a back-thinned 1340×1300 array with 20  $\mu\text{m}$  pixel size is used. To increase the flux density at the detector plane, a cylindrical Au mirror is set at a glancing angle of 4°, with its surface orthogonal to the flat-field grating. A limited aperture filter between the grating and detector discriminates against fluorescent and scattered emission within the spectrometer. The diffraction grating is located at a distance of 1.25 m from the target being imaged, and the detector plane is 0.235 m from the grating center. The view angle is 34° with respect to target rear side normal. The solid angle subtended by the spectrometer is  $5.69 \times 10^{-5}$  sr and spatial magnification is 0.6 (demagnification) giving a resolution of approximately 35  $\mu\text{m}$ .

XUV imaging at two photon energies (i.e., 68 and 256 eV) is also used. Each of the XUV imagers consists of a combination of spherical and planar multilayer mirrors.<sup>5</sup> The target rear surface emission is imaged onto the CCD array through a 90°-fold that isolates the CCD from direct target emission and allows for shielding against high energy photons (hard hits). Each spherical-plane mirror pair has match-

<sup>a)</sup>Contributed paper, published as part of the Proceedings of the 17th Topical Conference on High-Temperature Plasma Diagnostics, Albuquerque, New Mexico May 2008.

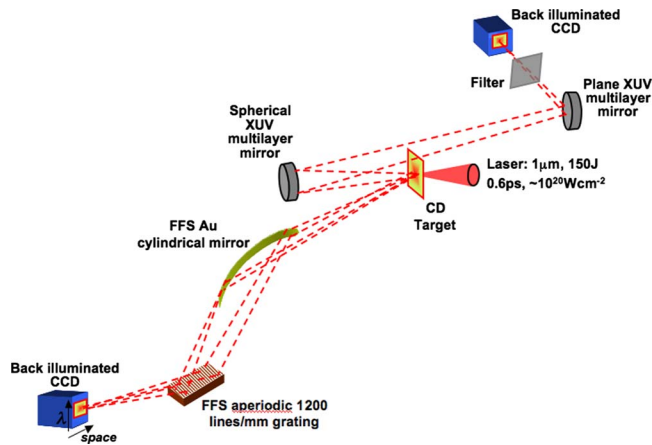


FIG. 1. (Color online) Schematic of the experimental setup.

ing spectral peaks and is optimized to image within a specific energy bandwidth. The spherical mirrors have a radius of curvature of 0.5 m, and are placed 27 cm away from the target, set at near normal incidence. The reflected image is deflected off the plane mirror and goes through a thin aluminum/polyimide filter, before reaching a CCD at a path length of 2.15 m. The total magnification of the system is 11 and the resolution is approximately  $9 \mu\text{m}$ . Further details can be found in Refs. 1 and 2.

### III. RESULTS AND DISCUSSION

The use of the cylindrical mirror in conjunction with the grating in the FFS allows for both spatial imaging and spectral imaging/dispersion. Indeed, for most targets, a double spectrum—one originating from the target rear plume, and one from the front plasma plume is seen in the flat-field data. Figure 2 shows spectra recorded on a single shot from both the front and rear side of the target (recorded with no low-pass filter). The spectrum shows a rear surface Planckian continuum with superimposed line radiation. The bright continuum is emitted from the high density, hot, optically thick rear surface of the solid target. As the lower density plasma plume forms on the back side and moves away from the surface, spectral lines become visible. The different falloff rates for the individual spectral lines are evidence for a plume changing in density and temperature as it expands from the surface. The spectra associated with the front surface plasma plume do not display any bright continuum, indicating that the plume visible on the front side from around the edge of the target is already of a low enough density to be optically thin to spectral lines in the XUV region.

Line radiation from an integrated region of roughly  $300\text{--}600 \mu\text{m}$  from the back surface and  $200\text{--}500 \mu\text{m}$  from the front surface of a  $25 \mu\text{m}$  CD planar target are identified. Populations of the carbon hydrogenlike (CVI) and carbon heliumlike (CV) ionic stages and their relative intensities are determined.

The atomic spectroscopy code FLYCHK (Ref. 6) is used to calculate line profiles of atomic transitions. FLYCHK uses a detailed level structure for lithiumlike, heliumlike, and hydrogenic ion stages to calculate charge state and population distributions. Spectra for densities between  $n_e = 1 \times 10^{18}\text{--}1$

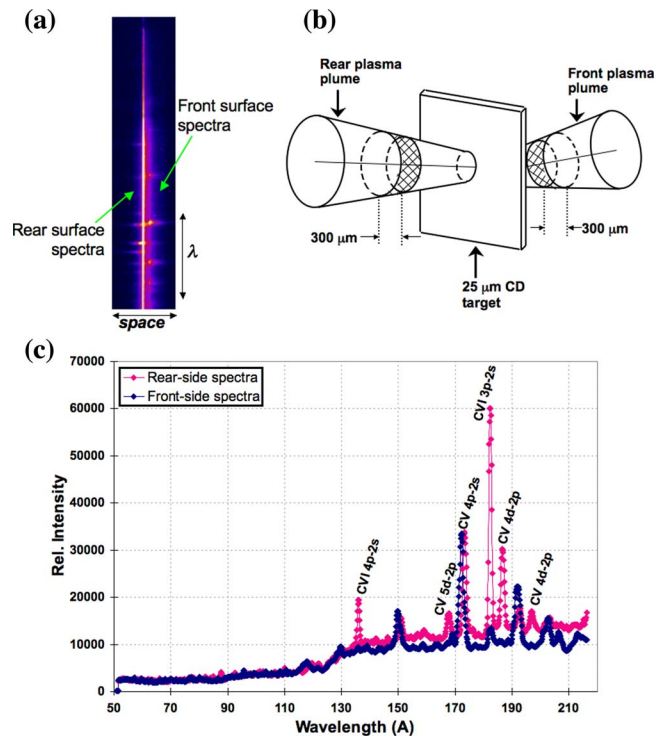


FIG. 2. (Color online) (a) The soft x-ray spectra for a CD planar target using a 1200 lines/mm diffraction grating. (b) Schematic illustration of the spatial zone from which plasma emission was recorded. (c) The lineouts for the front and rear surface spectra.

$\times 10^{21} \text{ cm}^{-3}$  and temperatures from  $10\text{--}1000 \text{ eV}$  are individually generated for both steady-state local thermodynamic equilibrium (LTE) and non-LTE conditions. In both cases, solutions are assumed to allow a single temperature and pressure to be attributed to the whole system for the sake of simplifying the problem. Line pair ratios of intensities of selected ionization transitions are determined from the synthetic spectra and then compared against the experimental spectra. It is found that at a given temperature, ratios do not significantly change for the different plasma densities. In both the LTE and non-LTE cases, it is assumed that the lines used for temperature measurements are not subject to reabsorption or induced emission.

The rear surface emission spectrum from a  $25 \mu\text{m}$  CD target irradiated at  $144 \text{ J}$ ,  $0.5 \text{ ps}$ , with a  $50 \mu\text{m}$  focal spot is analyzed. From the FFS, the experimental ratios of hydrogenic to heliumlike lines integrated over the region of  $300\text{--}600 \mu\text{m}$  from the back surface is determined: CVI  $4p\text{--}2s$  (Balmer beta,  $\lambda = 135 \text{ \AA}$ ) to CV  $4p\text{--}2s$  (heliumlike Balmer beta analog,  $\lambda = 173 \text{ \AA}$ ) is 0.3; CVI  $3p\text{--}2s$  (Balmer alpha,  $\lambda = 182 \text{ \AA}$ ) to CV  $4d\text{--}2p$  (heliumlike Balmer beta analog,  $\lambda = 187 \text{ \AA}$ ) is 2.5; and CVI  $3p\text{--}2s$  to CV  $5d\text{--}2p$  (heliumlike Balmer gamma analog,  $\lambda = 167 \text{ \AA}$ ) is 7.1. After comparison to synthetic spectra for plasma density  $n_e = 1 \times 10^{18} \text{ cm}^{-3}$  (the density at which the experimental spectrum most closely matches the synthetic spectrum shape), this predicts a plasma temperature of 67.6, 75.9, and 79.3 eV from each of the line pair ratios, respectively, in the LTE case, and plasma temperatures of 64.8, 78.5, and 80.2 eV in the non-LTE limit. Figure 3 compares the predicted line ratios with the experimental results. The average temperature of the rear

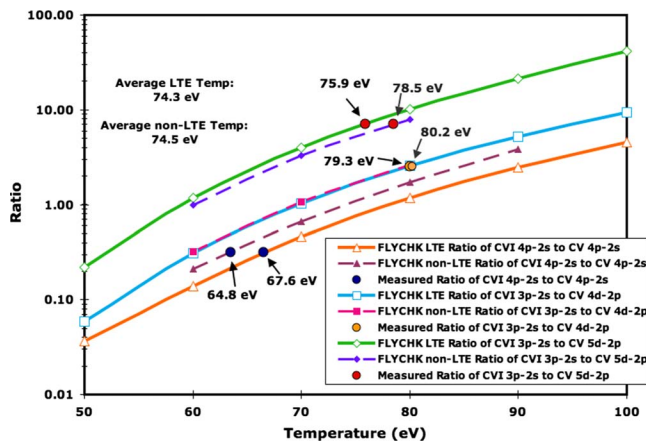


FIG. 3. (Color online) The comparison of measured experimental line pair ratios for spatial zone marked in Fig. 2 with expected line pair ratios generated using the FLYCHK spectroscopic code.

plasma plume of 300–600  $\mu\text{m}$  from the back surface is thus  $74.4 \pm 0.1$  eV, assuming minimal opacity effects.

Imaging using the XUV diagnostic offers a dual function: a qualitative high spatial resolution visual of the target heating, and a quantitative measurement of the initial target temperature at the rear surface. Taking into account the XUV multilayer mirror reflectivities, the collection solid angle, image magnification, detector quantum efficiencies, mirror bandwidths, and filter transmissions, an absolute time-integrated XUV brightness can be derived for each pixel of the image. This brightness can then be compared against LASNEX (Ref. 7) simulations which output an expected XUV brightness as a function of plasma temperature. Further details of the methodology for analyzing XUV images is found in Refs. 1 and 2. The 68 eV XUV imager and 256 eV XUV imager show pre-expansion peak temperatures of the rear surface of 127 and 154 eV, respectively, for the same 25  $\mu\text{m}$  CD target.

The temperatures calculated from the two XUV imagers, while fairly consistent with each other, are approximately 70 eV higher than the temperature predicted by the FFS (nearly a factor of 2). The XUV imager measurement is de-

rived from the optically thick continuum of the dense hot phase of the plasma, whereas the flat-field spectrum is taken from the low density plasma plume; thus, the lower temperature obtained represents an average over the cooling phase of the plasma.

If a pure adiabatic cooling of the plasma is assumed as it expands from the target rear surface, then based on a change in temperature of a factor of 2, it would be expected that the plasma would expand by nearly  $3\times$ . However, the spatial scaling of the flat-field spectra shows that the plasma expands far more, and thus there is evidence of frozen ionization that leads to an overestimation of the plume temperature.

To conclude, a comparison has been made of plasma temperature at the rear surface and in the rear plasma plume of the target using three methods. These techniques reveal more information about the three-dimensional plasma temperature and expansion characteristics.

## ACKNOWLEDGMENTS

The authors thank the Jupiter Laser Facility staff. This work was performed under the auspices of the U.S. Department of Energy by Lawrence Livermore National Laboratory under Contract Nos. DE-FG02-05ER54834, W-7405-Eng-48 No. DE-FC02-04ER54789 (Fusion Science Center), and DE-AC52-07NA27344. T. Ma is funded through LLNL's Institute of Laser Science and Applications grant.

- <sup>1</sup>P. Gu, B. Zhang, M. H. Key, S. P. Hatchett, T. Barbee, R. R. Freeman, K. Akli, D. Hey, J. A. King, A. J. Mackinnon *et al.*, *Rev. Sci. Instrum.* **77**, 113101 (2006).
- <sup>2</sup>T. Ma, A. G. MacPhee, M. H. Key, S. P. Hatchett, K. U. Akli, T. W. Barbee, C. D. Chen, R. R. Freeman, J. A. King, A. Link *et al.*, *Rev. Sci. Instrum.* (unpublished).
- <sup>3</sup>T. Tokushima, Y. Harada, M. Watanabe, Y. Takata, A. Hiraya, and S. Shin, *Surf. Rev. Lett.* **9**, 503 (2002).
- <sup>4</sup>D. Neely, A. Damerell, R. Parker, and M. Zepf, CLF Annual Report, 1994–1995.
- <sup>5</sup>T. W. Barbee, Jr., *Opt. Eng. (Bellingham)* **25**, 898 (1986).
- <sup>6</sup>H.-K. Chung, M. H. Chen, W. L. Morgan, Y. Ralchenko, R. W. Lee, *High Energy Density Phys.* **1**, 3 (2005).
- <sup>7</sup>G. Zimmerman, D. Kershaw, D. Bailey, and J. Harte, Inertial Confinement Fusion Conference, San Diego, CA, 1978 (unpublished).